ISSN 1070-3632, Russian Journal of General Chemistry, 2013, Vol. 83, No. 12, pp. 2260–2268. © Pleiades Publishing, Ltd., 2013.
Original Russian Text © L.B. Belykh, N.I. Skripov, V.V. Akimov, V.L. Tauson, T.P. Stepanova, F.K. Schmidt, 2013, published in Zhurnal Obshchei Khimii, 2013, Vol. 83, No. 12, pp. 1974–1983.

The State of Palladium in the Nanosized Hydrogenation Catalysts Modified with Elemental Phosphorus

L. B. Belykh[a], N. I. Skripov[a], V. V. Akimov[b], V. L. Tauson[b], T. P. Stepanova[a], and F. K. Schmidt[a]

[a] *Irkutsk State University, ul. K. Marksa 1, Irkutsk, 664003 Russia*
e-mail: belykh@chem.isu.ru

[b] *Vinogradov Institute of Geochemistry, Siberian Branch, Russian Academy of Sciences, Irkutsk, Russia*

Received June 25, 2012

Abstract—The size, nature, and surface state of nanoparticles formed by reduction of $Pd(acac)_2$ with hydrogen in the presence of P_4 have been elucidated by means of X-ray photoelectron spectroscopy, X-ray powder diffraction analysis, and transmission electron microscopy. The nanoparticles (average diameter of 5.6 nm) consist of Pd_6P and palladium nanoclusters (at initial ratio P/Pd = 0.3). Dimethylammonium dihydro- and hydrophosphates are found in the surface layer of the catalyst nanoparticles. The nanoparticles are stabilized by ammonium salts formed via dimethylformamide hydrolysis.

DOI: 10.1134/S1070363213120062

Elucidation of the features of formation, operation, and deactivation of the catalytically active particles is one of the most important fields of catalysis science. These problems have been discussed in a number of papers [1–6]. Although the fundamentals of catalysts preparation have been developed and known to date, no universal approach is known providing a catalyst with optimal activity, selectivity, and efficiency for any given process.

We have recently demonstrated that phosphines [7] as well as elemental phosphorus [8, 9] are efficient promotors for palladium catalysts of hydrogenation of unsaturated compounds, nitro derivatives, and aldehydes. The promoting effect of phosphorus depends on several factors, like the nature of the acyl ligand in the Pd precursor, the reducing agent used, the P/Pd ratio, and the catalyst concentration. The introduction of small amount of phosphorus (P/Pd < 0.7) before the stage of $Pd(acac)_2$ reduction with hydrogen enhances the turnover frequency and turnover number of the palladium catalyst [8]. The highest catalytic activity has been observed at P/Pd of 0.3. The turnover number of the so modified catalyst in the reaction of alkene hydrogenation [mild conditions, 30°C, $P(H_2)$ = 1 atm] is 9 times higher than that of the unmodified catalyst. With growing concentration of phosphorus, the promoting effect is decreasing, and at equimolar P/Pd ratio the catalytic activity is completely suppressed.

In order to elucidate the nature of the above-mentioned efficient catalyst of hydrogenation, in this work we studied the palladium sample prepared in the presence of elemental phosphorus (P/Pd = 0.3) by means of X-ray photoelectron spectroscopy (XPS), X-ray powder diffraction analysis (XRD), and transmission electron microscopy (TEM).

According to UV spectroscopy and TEM data, in the hydrogen medium at 80°C the $Pd(acac)_2$–0.3P system was quantitatively converted into acetylacetone and highly contrast particles (average diameter of 5.6±1.5 nm, Fig. 1) within 15–20 min.

The black precipitate isolated from the $Pd(acac)_2$–0.3P–H_2 reaction mixture was X-ray amorphous material. The diffuse halo in the XRD pattern was observed at 2θ of 35–45° (Fig. 2a); that range was characteristic of intense diffraction peaks of metal palladium [PDF 5-0681, (111) 2.246 Å] [10] as well as of Pd-enriched palladium phosphides, in particular, Pd_6P [PDF 19-882 (043, 023) 2.254 Å], $Pd_{4.8}P$ [PDF 19-0890, (023) 2.252 Å], Pd_7P_3 [PDF 31-936, (301) 2.254 Å], and $Pd_3P_{0.8}$ [PDF 42-922, (031) 2.255 Å] [10]. The coherent scattering domain size as calculated using the Scherrer equation [11] equaled 3.10±0.02 nm. The difference in the particles size as deduced from TEM and XRD could be due to several reasons. For

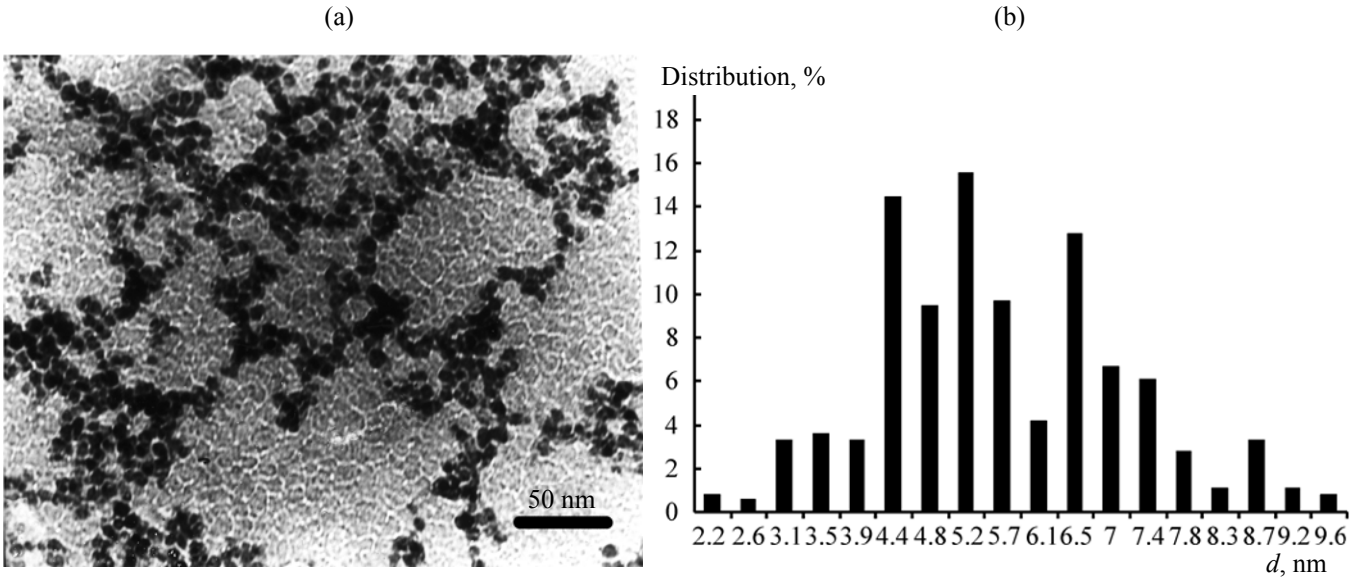

Fig. 1. Palladium catalyst modified with elemental phosphorus: TEM picture (a) and particles size distribution (b).

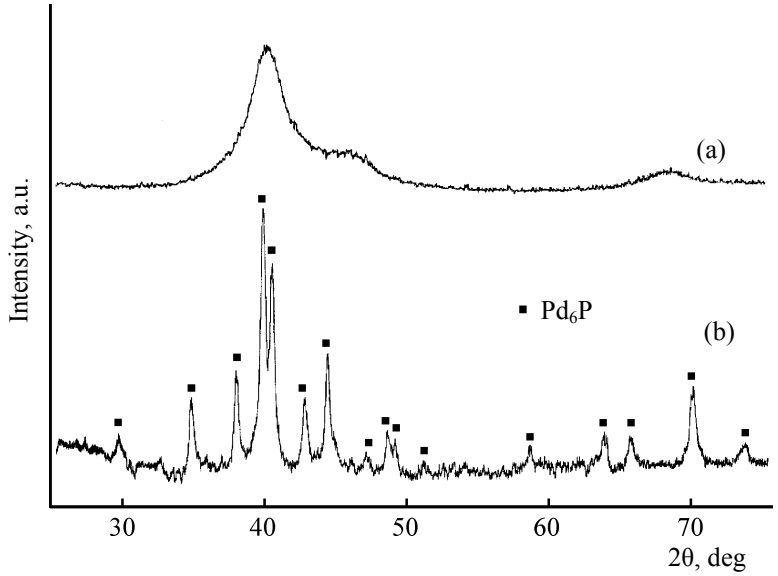

Fig. 2. XRD pattern of the specimen isolated from the $Pd(acac)_2$–0.3 P system, before (a) and after (b) calcination.

example, the coherent scattering domain size which is commonly assigned to the mean crystallite size was determined experimentally basing on the information on the diffraction reflection broadening. However, in addition to the particles size decrease below 100 nm, the diffraction lines could be broadened due to microstrains arising from the chemical inhomogeneity (segregation), structure imperfection [12].

From the elemental analysis data, the elemental formula of the catalyst was $Pd_{9.1}P_1C_{2.2}H_{6.7}O_{4.1}$. Most likely, carbon and hydrogen were included into the catalyst specimen in the form of solvent, dimethylformamide DMF. However, the content of oxygen (calculated as difference between 100% and sum of Pd, P, C, and H) was relatively high, thus, other oxygen compounds could be present in the sample besides DMF.

According to the phase diagram of Pd–P system [13], the $Pd_{15}P_2$ phosphide was the most enriched with palladium, however, Pd/P molar ratio in the studied specimen (9.1) was well above 15/2 = 7.5. Moreover, about 27% of reduced palladium was present in the

Binding energy and concentration of elements in various oxidation states in the surface layers of palladium catalyst

Spectral line	Binding energy, eV[a]	FWHM, eV	Element concentration, mol %	Most probable form[b]
Pd 3*d*	334.52	3.0	7.3	Pd^0 (0.55)
	(339.78)	3.0		
	336.28	3.0		Pd_xP (0.45)
	(341.54)	2.6		
	342.88	3.0		Pd_xP (Pd $3d_{5/2}$)[c]
	344.11	3.0		Pd^0 plasmon peak
	347.71	2.9		Pd_xP (P*d* $3d_{3/2}$)[c]
P 2*p*	129.51	3.0	3.7	Pd_xP (0.09)
	(130.31)	3.0		
	132.25	3.0		$(NH_2R_2)_2HPO_3$ (0.49)
	(133.05)	2.9		
	134.15	3.0		$(NH_2R_2)H_2PO_4$ (0.41)
	(134.95)	3.0		
	137.76	2.4		Pb ($4f_{7/2}$) admixture (<0.005)
N 1*s*	399.15	3.1	5.5	$HC(O)NR_2$ (0.11)
	402.22	4.0		$[NH_2R_2]_2HPO_3$, $[NH_2R_2]H_2PO_4$ (0.54)
	405.97	4.0		RNO_2 (0.35)
	408.55	2.8		$[NH_2R_2]_2HPO_3$,[c] $[NH_2R_2]H_2PO_4$[c]
O 1*s*	530.79	4.0	46.4	Pd(met.) $3p_{3/2}$ (0.22)
	532.06	4.0		$[NH_2R_2]_2HPO_3$, $[NH_2R_2]H_2PO_4$ (0.43)
	533.68	3.0		Pd_xP $3p_{3/2}$ (0.16)
	535.20	2.9		acacH (0.19)
	537.14	3.4		Pd(met.)[c] (Pd $3p_{3/2}$)
	539.84	4.0		Pd_xP (Pd $3p_{3/2}$)[c]
C 1*s*	283.70	3.8	37.10	acacH (C–C, C–H), $[NH_2R_2]$ (C–H) (0.35)
	285.01	2.1		Hydrocarbon impurities (0.01)
	286.82	4.0		$HC(O)NR_2$ (0.30)
	290.05	3.3		acacH (C=O) (0.21)
	292.37	3.8		CO_2, CO_3^{2-} (0.13)

[a] Binding energy of the second doublet line is given in parentheses. [b] Molar fraction of the respective form of the element is given in parentheses. [c] Satellites and shake-up lines.

sample (see Experimental section for the analysis procedure). After the studied sample was converted into the crystalline state, the diffraction maxima of Pd_6P were the only peaks observed in the XRD curve (Fig. 2b). The obvious disagreement between elemental analysis and XRD data was likely due to Pd^0 presence in the highly dispersed, X-ray amorphous state. Accounting for the total content of palladium and phosphorus, the fraction of reduced palladium, and palladium phosphide composition, the ratio of the Pd-containing components could be expressed as $[\{Pd_6P\}_{1.0}\{Pd(0)\}_{3.1}]$.

XPS study of the palladium catalyst revealed the presence of 5 elements (Pd, P, C, O, and N) in the surface layer of the sample. The ratio of the integral intensities of the respective signals is tabulated.

Spectra of all the five elements were complex, consisting of several components. In particular, modeling of the experimental Pd spectrum showed that it could be represented by a combination of seven lines, of which two pairs of the most intense peaks with binding energy of 334.52, 339.78 eV and 336.28, 341.54 eV could be assigned, respectively, to two spin-orbit doublets $3d_{5/2–3/2}$ corresponding to various chemical forms of palladium. The three weaker peaks with higher binding energy (342.9, 344.1, and 347.7 eV) were likely shake-up satellites and metal palladium plasmon peak (Fig. 3). The relative content of palladium forms is given in the Table.

The state of palladium in the bulk metal was reflected by the binding energy of *BE*(Pd $3d_{5/2}$) of 335.2 eV in XPS curve [14–16]. The lower binding energy as compared to bulk metal was observed in the case of Pd^0 in the dispersed state, with coordination number below 12 [16]. Therefore, the observed XPS peak at *BE*(Pd $3d_{5/2}$) of 334.5 eV could be reasonably assigned to Pd nanoclusters or nanofilms.

Some of the binding energies observed in Pd $3d_{5/2}$ spectra were higher as compared to that of the bulk metal, thus revealing the presence of some positive charge at Pd. According to [16, 17], the Pd $3d_{5/2}$ spectrum component of 336.3 eV could not be assigned to PdO [*BE*(Pd $3d_{5/2}$) = 336.8–337.0 eV]. The observed binding energy value was closer to that in palladium phosphides [*BE*(Pd $3d_{5/2}$) = 336.2 eV] [17]. Moreover, in the 2*p* spectrum of phosphorus consisting of seven lines (three P $2p_{3/2–1/2}$ spin-orbit doublets with P $2p_{3/2}$ maxima at 129.5, 132.2, and 134.2 eV and admixture of Pb $4f_{7/2}$ of 137.7 eV) (Fig. 4), the peak with *BE* = 129.5 eV was observed, typical of P $2p_{3/2}$ level in metal phosphides [18]. Therefore, the 336.3 eV peak in the Pd $3d_{5/2}$ spectrum could be reliably assigned to palladium phosphide. Taking into account the fractions of phosphorus and palladium (see table), the elemental formula of one of the surface compounds with binding energy of 336.3 eV (Pd $3d_{5/2}$) and 129.5 eV (P $2p_{3/2}$) could be represented as $Pd_{9.8}P$. The ratio of Pd/P, higher than that in the case of Pd-enriched phosphide $Pd_{15}P_2$, could be due to metal palladium clusters located on the surface of palladium phosphide particles; therefore, the concentration of palladium in the surface layer (about 3 nm, XPS spatial sensitivity) was overestimated.

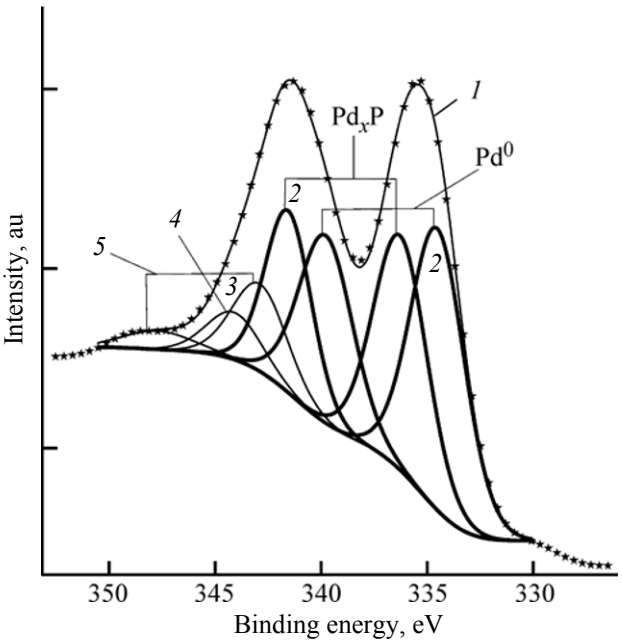

Fig. 3. XPS Pd 3*d* line of the palladium catalyst. (Asterisks) denote the smoothed experimental values, (*1*) sum of the XPS line components, (*2*) XPS line expansion into two palladium forms (Pd^0 and Pd_xP), Pd_xP satellites (*3*, *5*), and Pd^0 plasmon peak (*4*). The components of Pd $3d_{5/2–3/2}$ doublet lines are shown by brackets.

Thus, palladium was found in the two states on the surface of the studied material: in the form of palladium clusters and of Pd-enriched palladium phosphide.

Noteworthily, palladium phosphide was not the major phosphorus form in the surface layer of palladium catalyst; two other forms prevailed, characterized by the binding energy of 132.2 and 134.2 eV in the P $2p_{3/2}$ spectrum (see table). Those energies are typical of phosphorus in phosphorus acids [19], dihydro- and hydrophosphates [20, 21], phosphates [22], and hydrophosphites [23]. From the P $2p_{3/2}$ spectrum, it was reasonable to suggest that the components with binding energy of 132.2 and 134.2 eV corresponded to phosphorus in phosphoric and phosphorous acids that were formed in the redox reaction of $Pd(acac)_2$ with white phosphorus [8] and then adsorbed on the palladium nanoparticles.

$$3Pd(acac)_2 + 2P + 6H_2O = 3Pd^0 + 6Hacac + 2H_3PO_3.$$

According to XPS data, atoms of N and C were found at the sample surface along with Pd, P, and O

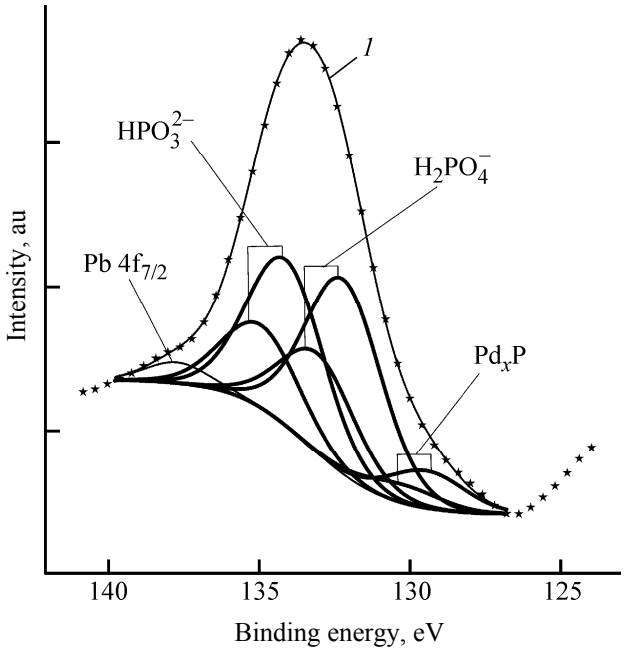

Fig. 4. XPS P 2*p* line of the palladium catalyst. (Asterisks) denote the smoothed experimental values, (*1*) sum of the XPS line components, (*2*) XPS line expansion into three phosphorus forms (Pd_xP, $H_2PO_4^-$, and HPO_3^{2-}). The components of P $2p_{3/2-1/2}$ doublet lines are shown by brackets.

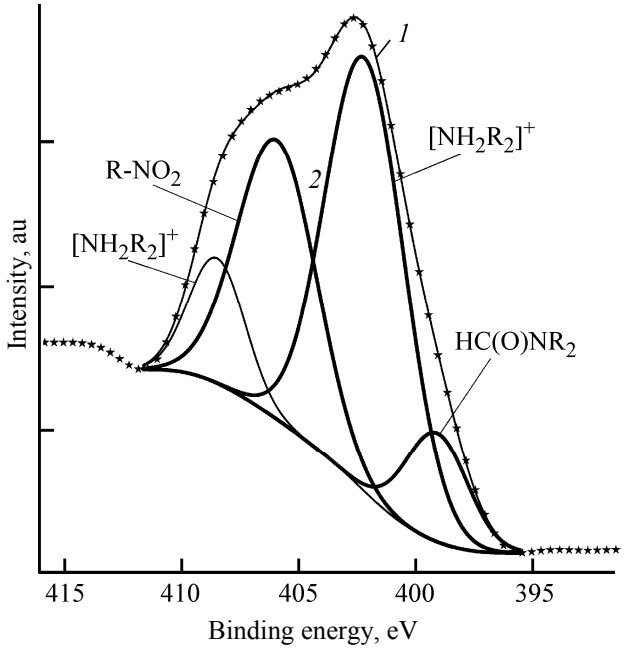

Fig. 5. XPS N 1*s* line of the palladium catalyst. (Asterisks) denote the smoothed experimental values, (*1*) sum of the XPS line components, (*2*) XPS line expansion into three nitrogen forms (DMF, its hydrolysis and oxidation products).

(see table). It should be noted that minor amounts (no more than 1 mol %) of carbon and oxygen are commonly found even on the surface of pure substances not containing these elements as a result of adsorption during the sample placement on the support. However, in this work higher concentrations of carbon and oxygen were detected, asserting that they were initially present in the sample.

The N 1*s* spectrum of the palladium catalyst was a combination of four lines with the maxima corresponding to the binding energy of 399.2, 402.2, 406.0, and 408.6 eV (Fig. 5). The peak of *BE*(N 1*s*) = 399.2 eV could be probably assigned to nitrogen in DMF, taking into account the N 1*s* binding energy in free acetamide (399.8 eV) and in coordinated acetamide (399.5 eV) [24]. Such assignment of the *BE*(N 1*s*) = 399.2 eV peak was consistent with the XPS analysis of the C 1*s* spectrum that contained a peak with *BE* = 286.8 eV (Fig. 6), typical of a carbon in substituted amides.

According to the N 1*s* spectrum, the major nitrogen form on the catalyst surface was that with the binding energy of 402.2 eV (see table) assigned to nitrogen in ammonium salts [20, 25–27]. Noteworthily, surface concentrations of nitrogen atoms with *BE*(N 1*s*) = 402.2 eV and phosphorus with *BE*(P 2*p*) of 132.2 and 134.2 eV were close to equimolar, $[P_\Sigma]/[N] = 1.1$ (see table).

Furthermore, a peak with *BE*(O 1*s*) = 532.1 eV was observed in the sample spectrum (Fig. 7), typical of oxygen in a hydroxy group of inorganic acids; additionally, a peak with binding energy of 283.7 eV was found in the C 1*s* spectrum (Fig. 6), corresponding to sp^3-carbon. The mentioned data led to reliable conclusion that the substituted ammonium dihydrophosphates, hydrophosphates, or hydrophosphites were located on the surface of the palladium catalyst.

As was previously confirmed, along with palladium dichloride reduction with hydrogen in DMF medium in the mild conditions (30°C, 1 atm), the solvent hydrolysis by water traces occurred, accelerated by the forming hydrochloric acid [9].

$$PdCl_2 + H_2 = Pd(0) + 2HCl,$$

$$HC(O)N(CH_3)_2 \xrightarrow{H_2O,\ HCl} HCOOH + NH(CH_3)_2,$$

$$HN(CH_3)_2 + HCl = [NH_2(CH_3)_2]Cl.$$

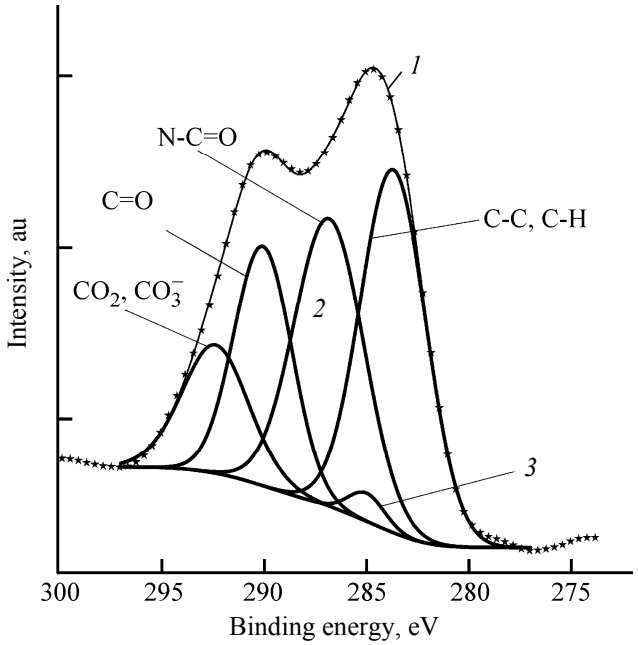

Fig. 6. XPS C 1*s* line of the palladium catalyst. (Asterisks) denote the smoothed experimental values, (*1*) sum of the XPS line components, (*2*) XPS line components assigned to the bonds in ammonium salts, acetylacetone, DMF, and poorly controlled hydrocarbon impurities (*3*).

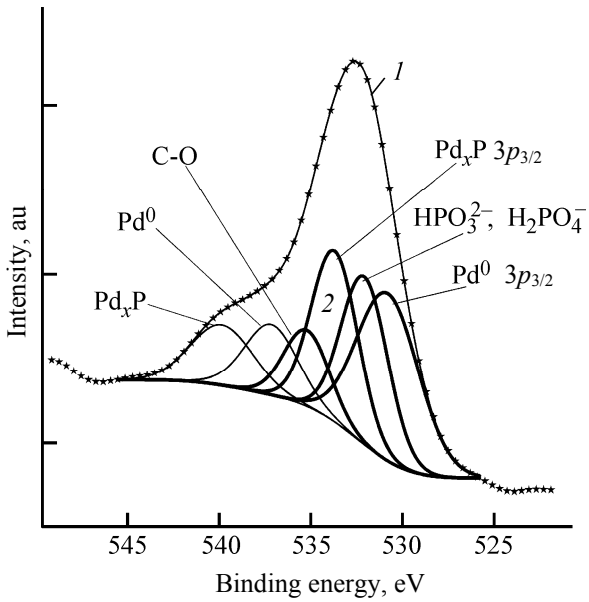

Fig. 7. XPS O 1*s* line of the palladium catalyst. (Asterisks) denote the smoothed experimental values, (*1*) sum of the XPS line components, (*2*) XPS line expansion into three oxygen forms ($H_2PO_4^-$, HPO_3^{2-}, and C–O). The C=O line is overlapped with Pd $3p_{3/2-1/2}$ satellite lines.

The data obtained in this work showed that the side reaction of DMF hydrolysis accelerated with phosphorus acids occurred in the course of palladium catalyst preparation from $Pd(acac)_2$ and elemental phosphorus in hydrogen atmosphere, leading to various substituted ammonium salts of phosphorus acids, for instance, $[NH_2(CH_3)_2]H_2PO_4$ or $[NH_2(CH_3)_2]_2HPO_3$. Ammonium compounds adsorbed on the surface could stabilize the nanoparticles by preventing their aggregation.

The N 1*s* peak with the binding energy of 406.2 eV is common of NO_2 group. Despite all possible measures taken, the oxygen traces could be present in hydrogen as well as in the solvents. It is known that metal palladium catalyzes hydrogen oxidation to hydrogen peroxide with the traces of oxygen [28]; subsequently, primary and secondary amines are oxidized into nitrocompounds and hydroxylamines, respectively, with H_2O_2 [29]. The observation of the peak with binding energy of 406.2 eV in the N 1*s* XPS spectrum led to the conclusion that such side processes accompanied the palladium catalyst preparation, thus changing the nanoparticles surface composition.

Acetylacetone could also participate in the particles stabilization, along with ammonium salts. The formation of acetylacetone via $Pd(acac)_2$ hydrogenolysis was evidenced by presence of the *BE*(C 1*s*) = 290.0 eV peak in the C 1*s* spectrum, characteristic of carbon of diketones carbonyl group (Fig. 6, table).

The study of palladium catalyst demonstrated that the nanoparticles prepared via reduction of $Pd(acac)_2$ with hydrogen in the presence of elemental phosphorus (P/Pd = 0.3) consisted of palladium phosphide Pd_6P and palladium nanoclusters. The obtained experimental data did not allow distinguishing between nanophases mixture and the core-shell structure. The XPS experimental data did not contradict the earlier suggested model of nanoparticles with palladium phosphide core and the catalytically active Pd clusters shell [8].

The data collected in this work along with the previously reported results [8, 9, 31] led to the following scheme of formation of nanosized palladium catalyst modified with elemental phosphorus in hydrogen medium (see Scheme 1).

Two reducing agents are present in the reaction mixture: hydrogen and elemental phosphorus. Bis(acetylacetonato)palladium is not reduced by hydrogen at 30°C, whereas its reaction with white phosphorus and the traces of water in the solvent occurs within 3–5 min at room temperature, to give phosphorous and phosphoric acids as well as phosphides PdP_2 and Pd_5P_2

Scheme 1.

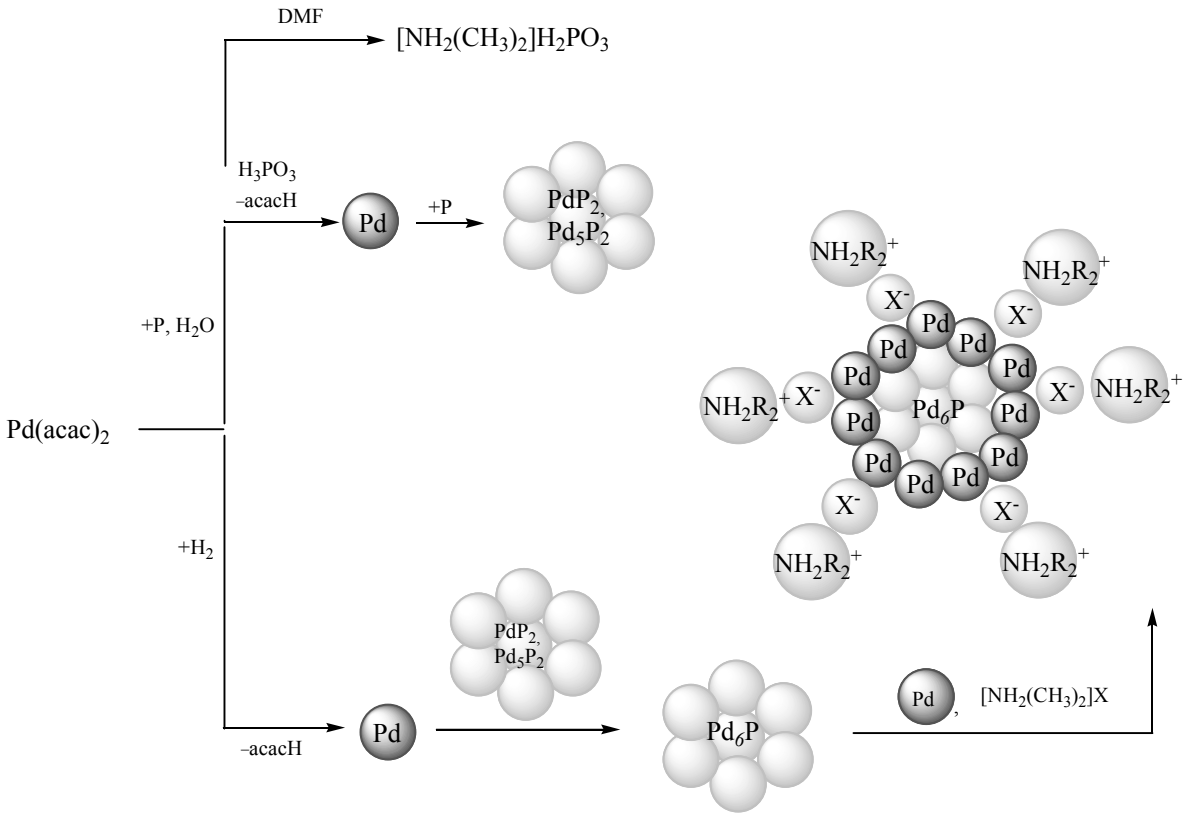

$X^- = H_2PO_3^-, H_2PO_4^-$.

[30]. The conversion of $Pd(acac)_2$ in the reaction with white phosphorus at P/Pd = 0.3 does not exceed 10%, thus, unreacted $Pd(acac)_2$ is present in the solution. The Pd^0 atoms formed as a result of the redox process interact with P_4, being transformed into phosphides PdP_2 and Pd_5P_2. Model study of the phosphides formation in the reaction of Pd^0 complex [$Pd(dba)_2$, dba = dibenzylideneacetone] with white phosphorus has revealed that at the initial stage the PdP_2 phosphide is formed, and its subsequent interaction with Pd(0) leads to Pd-enriched phosphides [31]. The latter act as centers of crystallization in the course of heterogeneous nucleation of Pd^0 clusters occurring at further stages of the unreacted $Pd(acac)_2$ reduction with hydrogen at 80°C.

EXPERIMENTAL

Solvents (benzene and DMF) were purified according to common procedures accepted in organometallic chemistry [32]. DMF was kept over anhydrous copper sulfate (in order to dry and to remove the amines impurities) till the solution turned green, and then it was twice distilled in a vacuum (8 mm Hg) avoiding heating above 42°C. Benzene was additionally distilled over $LiAlH_4$ in the rectification column, and then stored under argon in sealed ampules over molecular sieves 4 A. Concentration of water (the Fischer's method [33]) was 1.1×10^{-3} mol/L (benzene) and 0.8 mol/L (DMF).

Bis(acetylacetonato)palladium was prepared according to [34]. ^{1}H NMR spectrum (benzene); δ, ppm 5.04 s (1H, CH), 1.76 s (6H, CH_3).

White phosphorus was mechanically cleaned of the oxidation products and washed with anhydrous benzene prior to use. Solution of white phosphorus in benzene was prepared and stored under inert atmosphere, in a vessel allowing evacuation and the subsequent filling with argon. ^{31}P NMR spectrum: δ_P –522 ppm.

The catalyst was prepared in a glass temperature-controlled vessel in a hydrogen atmosphere, at 80°C. 2 mL of phosphorus (5.1×10^{-4} mol) solution in benzene was added dropwise to a solution of 0.51748 g (1.7×10^{-3} mol) of $Pd(acac)_2$ in 60 mL of DMF under

hydrogen (P/Pd = 0.3). The reaction mixture was stirred at 25°C during 5 min, at hydrogen pressure of 1 atm 1 min after white phosphorus solution addition, the yellow color turned into dark-brown. The reaction mixture was then heated to 80°C and further stirred during 15 min under excessive pressure of hydrogen (1 atm). After that, the conversion of $Pd(acac)_2$ was complete, according to UV data. The black-brown solution was cooled to ambient temperature. After evaporation of 2/3 of the solvent, benzene was added till the formation of the precipitate. The precipitate was washed with 10 mL of benzene three times under argon and dried (50°C, 1 mm Hg). Yield 0.19 g. IR spectrum at 4000–400 cm^{-1} revealed no absorption bands. Found, %: Pd 87.88, P 3.59, C 0.99, H 0.25.

The sample was X-ray amorphous. Diffuse halo was observed at 2θ 35°–45°, coherent scattering domain size of 3.10±0.02 nm. The sample was crystallized via calcination at 400°C during 4 h in the inert atmosphere. XRD, d/n (I/I_0): 2.993(13), 2.570(30), 2.362(40), 2.259(100), 2.225(78), 2.210(30), 2.037 (45), 2.010(10), 1.926(9), 1.868(17), 1.852(15), 1.784 (7), 1.573(12), 1.456(14), 1.419(14), 1.342(31), 1.284 (10), 1.244(4) Å (Pd_6P) [10].

Palladium(0) concentration was determined after its oxidation with iodobenzene [35]. The subsequent interaction of PdI_2 with NBu_4I led to the formation of $(NBu_4)_2[PdI_4]$. The $[PdI_4]^{2-}$ anion was quantitatively determined by UV spectrophotometry.

$$Pd(0) + PhI = Pd(Ph)I,$$

$$2Pd(Ph)I = Ph – Ph + PdI_2 + Pd(0),$$

$$PdI_2 + 2NBu_4I = (NBu_4)_2[PdI_4].$$

It was demonstrated that palladium phosphides were inert in those reactions.

To determine Pd^0 concentration, a solution containing 2×10^{-5} mol of Pd in 10 mL of DMF was put into a temperature-controlled vessel filled with argon, and 0.1477 g (0.4 mmol) of NBu_4I and 0.109 mL (1 mmol) of iodobenzene were added. The reaction mixture was stirred with a magnetic stirrer at 80°C till $[PdI_4]^{2-}$ concentration was constant. $[PdI_4]^{2-}$ concentration was determined on a VSU2-P spectrophotometer using the absorption band at 340 nm (ε_{340} = 23750 L cm^{-1} mol^{-1}) in a fused quartz cell with 0.1 cm optical path.

XPS studies were performed with Riber LAS-3000 photoelectron spectrometer. Before admission to the spectrometer, the sample was crushed in the agate mortar and applied to a conductive carbon tape. The spectrum was excited with polychromatic AlK_α X-ray irradiation (1486.6 eV). Photoelectron spectra were registered at the chamber pressure of 6.7×10^{-10} mbar. The qualitative composition of the surface was estimated from the general spectrum at 0–1100 eV with 1 eV data spacing, at the analyzer transmission energy of 50 eV. Quantitative composition of the surface and the forms of the elements were deduced from the precise spectra of the separate lines with 0.1 eV data spacing and the analyzer transmission energy of 25 eV. The analyzer was calibrated according to the Au $4f_{7/2}$ and Cu $2p_{3/2}$ lines at 84.0 eV and 932.7 eV, respectively.

The usual method of narrow spectra calibration with the internal standard (C 1*s* or Pd $3d_{5/2}$ line) was hardly possible due to the presence of several prevailing chemical forms with unknown binding energy. Therefore, the C 1*s* spectral line was registered under similar conditions, using a reference sample containing no carbon. Intensity and position of hydrocarbons C 1*s* line was thus determined (285.15 eV). Then, the binding energy scale of narrow XPS spectra of the catalyst was shifted by –0.15, and the component with binding energy of 285.0 eV was accounted for in the series expansion of the C 1*s* line. The experimental data were processed applying the CasaXPS software. The Pd $3d_{5/2–3/2}$, and P $2p_{3/2–1/2}$ doublet lines (spin-orbit splitting) were fitted with two Lorentz-Gauss curves with the interdoublet spacings of 5.26 and 0.84 eV, respectively, and fixed area ratio: 2/3(Pd $3d_{5/2–3/2}$) and 1/2(P $2p_{3/2–1/2}$). The full width of the spectral lines at half-maximum intensity (FWHM) was refined in the range of 2 to 4 eV. If FWHM was above 4 eV, such line should be a composite one, due to several chemical forms of an element. The difference in the doublet lines FWHM was below 0.4 eV. The O 1*s* line overlapped with Pd $3p_{3/2}$ line, therefore, the number of palladium chemical forms and their lines location was consistent with the second doublet line Pd $3p_{1/2}$ in the low-resolution (general) spectrum.

XRD studies were performed with DRON-3M diffractometer (CuK_α).

TEM studies were preformed with Philips EM-410 microscope. A droplet of the solution of *in situ* formed catalyst was put onto the supporting carbon-covered grid, and dried in an argon atmosphere. Under the registration conditions, specimen melting or

decomposition under the electron beam did not occur. The size distribution chart was obtained by analysis of a region containing no less than 500 high-contrast particles.

ACKNOWLEDGMENTS

This work was financially supported by the Ministry of Education of the Russian Federation (no. 14.B37.21.0795) and by Irkutsk State University (no. 2012-03-03).

REFERENCES

1. Navalikina, M.D. and Krylov, O.V., *Russ. Chem. Rev*., 1998, vol. 67, no. 7, p. 587.
2. Molnar, A., Sarkany, A., and Varga, M., *J. Mol. Catal*., 2001, vol. 173, no. 1–2, p. 185.
3. Nagaveni, K., Gayen, A., Subbanna, G.N., and Hegde, M.S., *J. Mater. Chem*., 2002, vol. 12, p. 3147.
4. Bonnemann, H. and Richards, R.M., *Eur. J. Inorg. Chem.,* 2001, vol. 2001, no. 10, p. 2455.
5. Ito, K., Ohshima, M., Kurokawa, H. Sugiyama, K., and Miura, H*., Catalysis Commun*., 2002, no. 3, p. 527.
6. Schmidt, F.K., *Kataliz kompleksami metallov pervogo perekhodnogo ryada reaktsii gidrirovaniya i dimerizatsii* (Catalysis with Metal Complexes of the First Transition Series of Hydrogenation and Dimerization Reactions), Irkutsk: Irkutsk. Gos. Iniv., 1986.
7. Schmidt, F.K., Belykh, L.B., and Goremyka, T.V., *Kinet. Catal*., 2003, vol. 44, no. 5, p. 623.
8. Belykh, L.B., Skripov, N.I., Belonogova, L.N., Umanets, V.A., and Schmidt, F.K., *Kinet. Catal*., 2010, vol. 51, no. 1, p. 42.
9. Skripov, N.I., Belykh, L.B., Belonogova, L.N., Umanets, V.A., Ryzhkovich, E.N., and Schmidt, F.K., *Kinet. Catal*., 2010, vol. 51, no. 5, p. 714.
10. *Powder Diffraction File. Q. Hanawalt Search Manual Inorganic Phases. JCPDS*, 1992.
11. Kitaigorodskii, A.I., *Rentgenostrukturnyi analiz* (X-Ray Analysis), Moscow: Tekh. Teor. Literatury, 1950.
12. Lipson, H. and Steeple. H., *Interpretation of X-Ray Powder Diffraction Patterns*, London: Macmillan, 1970.
13. Okamoto, H., *J. Phase Equilibria*., 1994, vol. 15, no. 1, p. 58.
14. Briggs, D. and Seah, M., *Practical Surface Analysis*, Ney York: John Wiley & Sons, 1990.
15. Moulder, J.F., Stickle, W.F., Sobol, P.E., and Bomben, K.D., *Handbook of X-Ray Photoelectron Spectroscopy*. Eden Prairie: Perkin-Elmer, 1992.
16. Tsyrul'nikov, P.G., Afonasenko, T.N., Koshcheev, S.V., and Boronin A.I., *Kinet. Catal*., 2007, vol. 48, no. 5, p. 728.
17. *Successful Design of Catalysts,* Inui, T., Ed., Amsterdam: Elsevier Science Publishers, 1988, p. 3.
18. Nemoshkalenko, V.BV, Didyk, V.V., Krivitskii, V.P., and Senkevich, A.I., *Zh. Neorg. Khim.,* 1983, vol. 28, no. 9, p. 2182.
19. Swift, P., *Surf. Interface Anal*. 1982, vol. 4, p. 47.
20. Le Bloa, A., Hbib, H., Bonnaud, O., Meinel, J., Quemerais, A., and Marchand, R., *Revue Phys. Appl.,* 1989, vol. 24, p. 545.
21. Bertrand, P.A., *J. Vac. Sci. Technol*., 1981, vol. 18, p. 28.
22. Gresch, R., Mueller-Warmuth, W.,and Dutz, H., *J. Non-Cryst. Solids*., 1979, vol. 34, p. 127.
23. Fluck, E. and Weber, D., Z. Naturforsch., 1974, vol. 29, p. 603.
24. Salyn', Ya.V., Nefedov, V.I., Mairova, A.G., and Kuznetsova, G.N., *Zh. Neorg. Khim.,* 1978, vol. 23, no. 9, p. 829.
25. Lindberg, B.J. and Hedman, J., *Chem. Scr*., 1975, vol. 7, p. 155.
26. Konno, H. and Yamamoto, Y., *Bull. Chem. Soc. Japan*, 1987, vol. 60, p. 2561.
27. Carley, A.F., Davies, P.R., and Mariotti, G.G., *Surface Sci*., 1998, vol. 401, p. 400.
28. Moreno, T., Garsia-Serna, J., Plucinski, P., Sanchez-Montero, M.J., and Cocero, M.J., *Appl. Catal. (A),* 2010, vol. 386, p. 28.
29. *Basic Principles of Organic Chemistry*, Roberts, J.D. and Caserio, C., Eds., New York, 1964.
30. Belykh, L.B., Skripov, N.I., Belonogova, L.N., Rokhin, A.V., and Schmidt, F.K., *Russ. J. Gen. Chem*., 2009, vol. 79, no. 1, p. 92.
31. Skripov, N.I., Belykh, L.B., Belonogova, L.N., Rokhin, A.V., Stepanova, T.P., and Schmidt, F.K., *Russ. J. Gen. Chem*., 2012, vol. 82, no. 2. P., 206.
32. Gordon, A.J. and Ford, R.A., *The Chemist's Companion. A Handbook of Practical Data, Techniques and References*, New York: Wiley, 1972.
33. Mitchell, J. and Smith, D.M., *Aquametry*, New York: Wiley, 1977.
34. USA Patent no. 3474464, 1969, *Ref. Zh. Khim*., 1970, 19N102P.
35. Schmidt, A.F. and Mametova, L.V., *Kinet. Catal*., 1996, vol. 37, no. 3, p. 406.